PROGRESS IN ELECTRICAL ENGINEERING
Vol. 1, No. 1, 2020, 55-76

URL : www.arfjournals.com

OPTIMAL DESIGN OF HEAT DISSIPATION STRUCTURE OF MFT CONSIDERING HIGH-FREQUENCY INSULATION PERFORMANCE

Yikun Zhao[1,2], Guoqiang Zhang[1,2], Dong Han[1,2], Kang Li[1,2], Zongjia Qiu[1] and Fuyao Yang[3]

[1]*Institute of Electrical Engineering, Chinese Academy of Sciences, Beijing, 100190, China*
[2]*University of Chinese Academy of Sciences, Beijing, 100039, China*
[3]*Global Energy Interconnection Research Institute, State Grid Corporation of China, Beijing, 102209, China*

Received: 9 April 2020 / Revised: 16 April 2020 / Accepted: 26 May 2020 / Published: 25 August 2020

Abstract: Although the increase in frequency improves the transmission efficiency of medium-frequency transformer (MFT), the heating problems of MFTs are more serious than conventional power transformers due to the increase in core losses and winding losses.Insulation performance and volume are important factors to be considered when designing heat dissipation structures. After testing the insulation properties of gas-solid insulation system at 1~20 kHz, the minimum internal insulation size of the resin-cast MFT wasproposed to avoid breakdown or flashoverfailures during the expected operating life.Subsequently, a natural air-cooled heat dissipation structurewasdesigned for the MFT model based on the accurate calculation of core losses, winding losses and surface heat transfer coefficients.Finally, the forced air-cooling heat dissipation method was studied to meet the application of smaller volume MFTs on the basis of ensuring the high-frequency insulation performance. The results show that, it's important to design the rational insulation structure of MFTs because the breakdown and flashover voltages of gas-solid insulating system are noticeable affected by frequency. The natural air-cooling method with heat sink fins on the upper and lower sides can limit the temperature rise of MFT to the allowable range for a 200 kVA, 10kHz MFT, while the forced air-cooling method with the air velocity of 1.6 m/s needs to be used if a smaller volume is required.

Index Terms: Medium-frequency transformer (MFT), heat dissipation, insulation properties, optimal design, gas-solid system.

I. INTRODUCTION

The power electronic transformer (PET), or solid-state transformer, was conceived as a replacement for the conventional power transformer. Reduction of weight and

This work was supported in part by the National Key R&D Program of China under Grant 2017YFB0903902.
Corresponding author: G. Zhang (*E-mail: zhanggqi@mail.iee.ac.cn*)

volume, improvement in efficiency, together with implement functions such as reactive power compensation, power flow control and integration of large-scale renewable energy are driving industrial and academic research in PET [1-3]. Medium-frequency transformers (MFTs) are key components of PET, which play an important role in power transmission and electrical isolation [4, 5]. At present, a series connection or parallel connection of multiple 1~100 kVA MFTs are used in large-capacity applications of PET, and the complicated structure brings about the problems of series voltage-sharing and parallel current-sharing. An effective solution is to develop high-capacity high-voltage MFTs that can replace the original series or parallel scheme [6]. However, the increase in the rated frequency leads to an increase in the loss density, which causes the heat generation of MFTs to be much higher than that of the power frequency transformers, and the breakdown properties of insulating materials are noticeable affected by frequency [7, 8]. Meanwhile, the smaller size and higher frequency of MFT add difficulties to the design of heat dissipation and insulation structure. Therefore, the design of large-capacity MFTs needs to consider the synergistic optimization of multiple factors including the volume of MFT prototypes, heat dissipation and insulation performance.

At present, design of MFTs is tied to many challenges compared to their traditional and technologically mature counterparts, such as power transformers and electronic transformers. Therefore, many studies around loss calculation, heat dissipation method and insulation structure design of MFTs have been carried out. In terms of loss calculation, the modified Steinmetz methods were gradually proposed to calculate the core losses at medium-frequency non-sinusoidal voltages, such as the modified Steinmetz equation (MSE) [9], generalized Steinmetz equation (IGSE) [10] and waveform coefficient Steinmetz equation (WCSE) [11]. Meanwhile, the Dowell model is considered by researchers to be a reasonable calculation method for the winding losses of MFTs [12]. Based on the accurate calculation of the loss density and the heat generation, some studies have been carried out around different heat dissipation methods of large-capacity MFTs. M. Mogorovic*et al* optimized the design of a 100 kVA/10 kHz MFT, using the natural air-cooling method with fin heat sink to reduce the steady-state temperature rise of the core to 75 K, while reducing the temperature rise of the windings to 122 K [7, 13]. After accurate calculation of the loss density of ferrite and nanocrystalline core, G. Ortiz verified the feasibility of forced air-cooling and water-cooling as the heat dissipation methods for MFTs with the rated parameter of 166 kVA/20 kHz [14]. For the oil-immersed MFT with a capacity of 1 MVA, T. Kjellqvist designed a prototype based on the oil-cooling system, which has additional problems such as oil leakage and flammability [15]. However, insulation structures of the above MFTs were designed with reference to the power frequency transformers, although the volume and heat dissipation performance of MFTs were optimized, the effects of frequency and volume limitation on insulation performance were not considered.

In addition, some studies have shown that both frequency and waveform types have noticeable effects on the insulation properties of gas-solid systems,and the original design method of power frequency transformers cannot be fully applied to the insulation design of MFTs [16-19]. Therefore,the premise of optimizing the heat dissipation structure is to ensure the insulation performance at high frequency, which should be determined by a large number of repetitive high-frequency insulation tests on insulating materials before the reliable insulation design standard of MFTs is proposed.

In this paper, we determined the minimum internal insulation size of the resin-cast MFT according to the breakdown properties of insulating materials and flashover properties of gas-solid system under high frequency square waveform. Then, a natural air-cooled heat dissipation structure was designed for the MFT model based on the accurate simulation calculation of core losses, winding losses and surface heat transfer coefficients. Finally, the reasonable air velocity in the forced air-cooling heat dissipation method was determined to meet the application of smaller volume MFTs on the basis of ensuring the high-frequency insulation performance.

II. INSULATION PROPERTIES OF GAS-SOLID SYSTEM

A. Platform for Insulation Tests

Fig. 1 shows the experimental platform for insulation tests at high frequencies, which is mainly composed of five parts: a) Power source with the adjustable output frequency, which is connected to the electrode device. b) Electrode device for performing the breakdown and flashover tests of insulating materials and air gaps. c) Voltage probe for detecting the high-frequency square waveform with the maximum measurable voltage of 40 kV. d) Current transducer for measuring the transient overcurrent. e) Digital oscilloscope with a bandwidth of 300 MHz for the acquisition of signal parameters. Among them, the power source can output bipolar square waveform signals with the frequency range of 1-20 kHz to simulate the actual operating conditions of MFTs. The high-frequency experimental platform can measure the insulation properties of insulating materials and air gaps at high frequencies, which can provide a reference for the insulation structure design of MFTs.

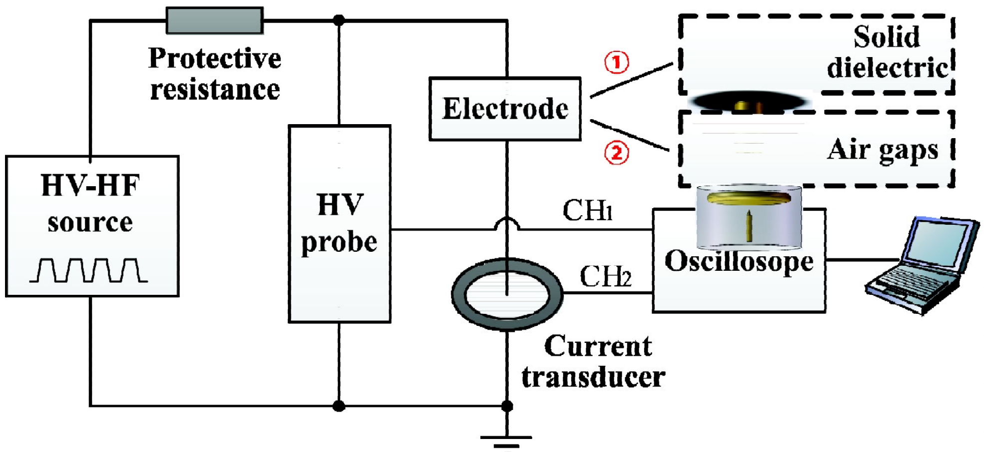

Figure 1: Experimental platform for the breakdown and flashover tests under high-frequency high-voltage signal

B. Breakdown Characteristics

Insulating materials widely used in transformers were selected as the samples, the thickness of which are the most commonly used in the insulation structures. According to the test results shown in Fig. 2, the short-time breakdown voltages drop remarkably with the increase of frequency. When the frequency is raised from 50 Hz to 20 kHz, breakdown voltages of insulating materials decrease to 27.8%~35.5% of original values. The noticeable reduce in breakdown properties is main caused by high-frequency thermal effect, which is closely related to the variations of dielectric loss factor tan δ and the dielectric constant ε. We have already analyzed the high-frequency thermal breakdown mechanism in the literature [8]. In addition, a constant stress breakdown test was performed at a frequency of 1 kHz~20 kHz. As an example, *V-t* characteristic curves of DMD insulation paper is shown in Fig. 3. It can be seen from Fig. 3 that the *V-t* characteristic curves of dielectric decrease with the increasing voltage frequency, indicating that the insulation life of the dielectric decreases at high frequencies.

In order to study the effect of voltage frequency on the insulation aging of dielectric, the surface condition of DMD insulation paper samples was observed under a scanning electron microscope (SEM) after a withstand voltage test at 4 kV for 20 minutes, as shown in Fig. 4. It can be seen from Fig. 4 that the increase in frequency makes the dielectric more damaged by the electrical stress during the same aging time, resulting in a decrease in insulation life. After 20 minutes of

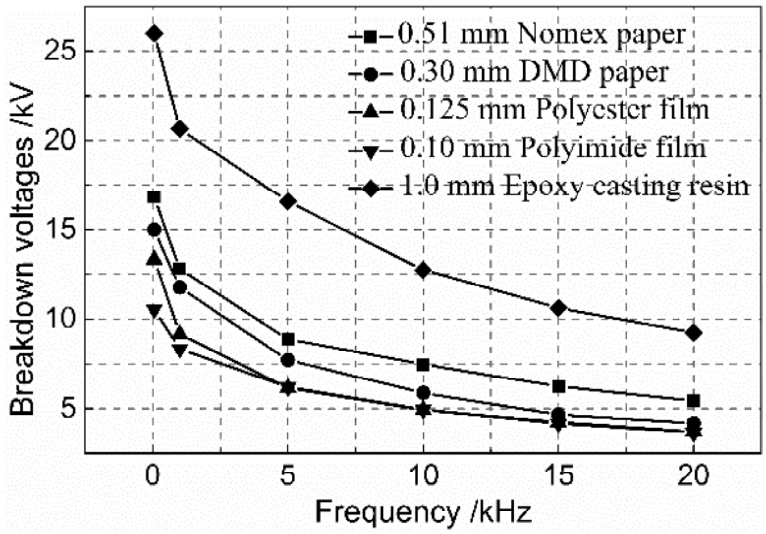

Figure 2: The variations of 1min breakdown voltages with frequency for the insulating materials widely used in transformers

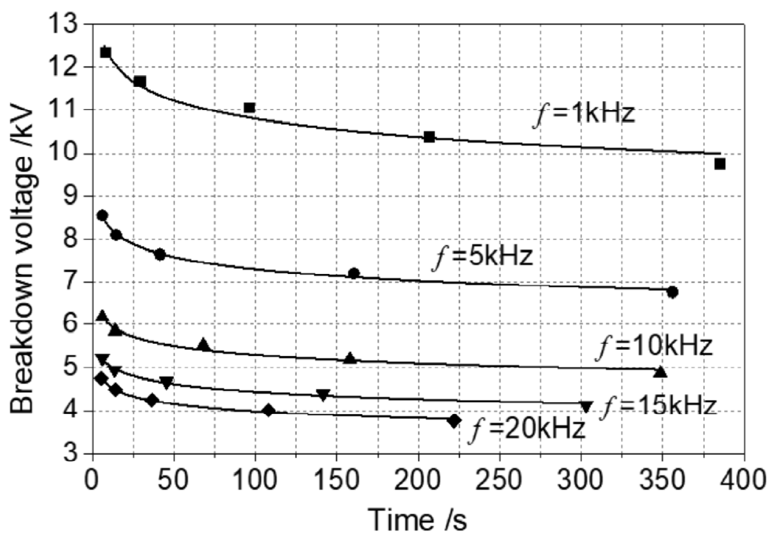

Figure 3: The *V-t* characteristic curves of 6641F type of DMD insulation paper under high frequency square waveform

withstand voltage test under the electrical stress of 4 kV/1 kHz, the internal fiber structure hardly changed, while part of the fiber structure is destroyed when the frequency is increased to 5 kHz. When the frequency is increased to 10 kHz, most of the fiber structure breaks and the probability of breakdown increases. Therefore, the winding insulation level should be set according to the rated frequency and rated voltage of the MFT to ensure that no insulation failure occurs during the expected insulation life. Table I lists the calculation results of the required insulation levels of MFTs with different rated parameters with an expected life of 20 years, which provides a reference for the design of the MFT internal insulation structure and the 1min withstand voltage tests.

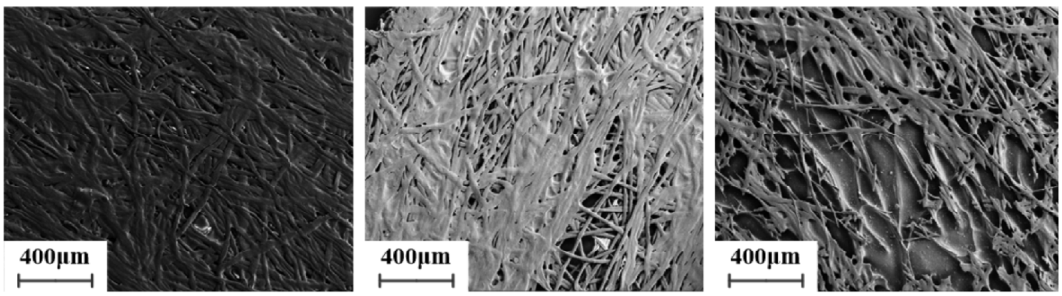

Figure 4. The conditions of DMD insulation paper under SEM after a withstand voltage test for 20 minutes. (a) 4kV/1kHz. (b) 4kV/5kHz. (c) 4kV/10kHz

Table I
Recommended Insulation Levelsof Windings for MFTs

Rated voltage (kV)	*Maximum voltage (kV)*	*Required insulation levels for different rated frequencies (kV)*			
		5 kHz	*10 kHz*	*15 kHz*	*20 kHz*
1.0	1.2	4.0	4.1	4.2	4.3
2.0	2.4	8.0	8.2	8.4	8.5
3.0	3.6	12.0	12.3	12.5	12.8
5.0	6.0	20.0	20.6	20.9	21.3
10.0	12.0	40.1	41.2	41.8	42.6
20.0	24.0	80.2	82.3	83.5	85.2

The breakdown of air gaps is one of the main reasons for the insulation failures of transformers, and is also an important part of the internal insulation design of MFTs. Fig.5 shows the test results of air gaps at high frequencies, which are consistent with standard IEC 60664-4 [20]. Although the breakdown strengths of the air gaps are hardly affected by frequency, the breakdown damages of electrodes are more

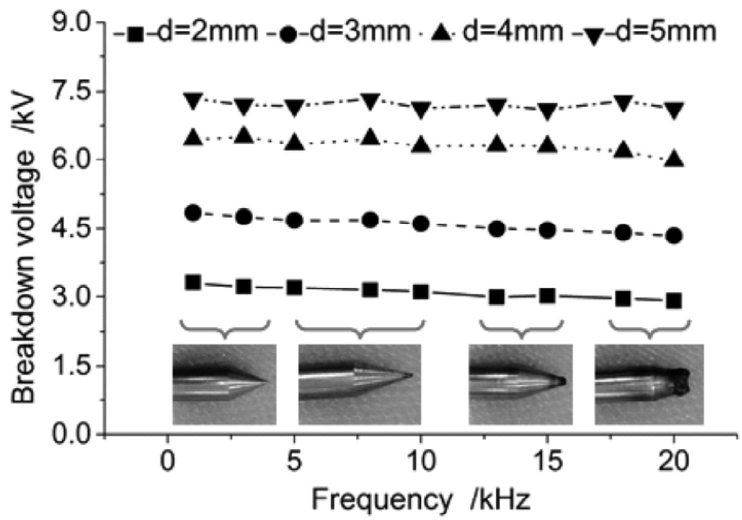

Figure 5: The breakdown characteristic of airgaps and the ablation of the needle electrodes after single breakdown test

serious as the frequency increases. Therefore, the insulation thicknesses of the air gaps and insulating materials should be increased when designing insulation structures of MFTs.

C. Flashover Characteristics

In order to reduce the probability of flashover between the core and windings, flashover tests were performed on the gas-solid insulation system. Before the tests, epoxy casting resin samples were cleaned with alcohol and then dried for 24 hours at 60 °C in a vacuum oven to remove impurities and moisture. Fig.6 shows the variation of flashover voltages with frequency, indicating that flashover voltages are reduced as the frequency increases. When the frequency raises from 1 kHz to 20 kHz, the flashover voltages of dielectrics decreases to 71.5% of original values. Therefore, the creepage distance should be increased to prevent the flashover between the core and windings in MFTs.

III. MFT MODELING

A. Internal Insulation Structure

Fig. 7 shows the schematic diagram of an epoxy casting MFT, in which the main structural parameters are defined. The material of core is selected as the

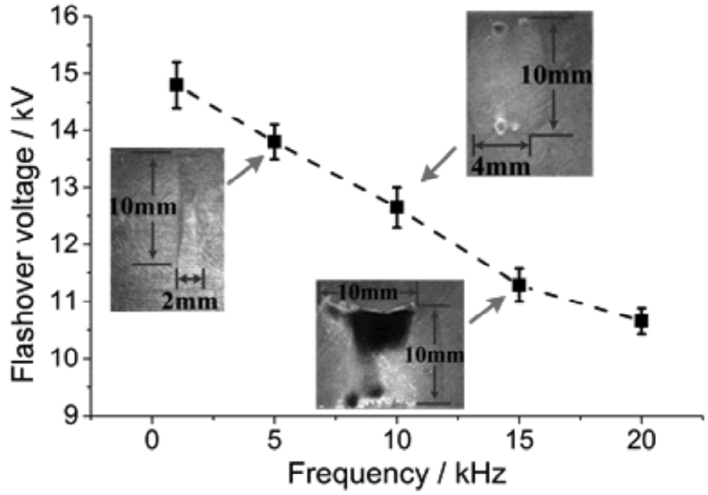

Figure 6: The variations of flashover voltages with frequency for gas-solid system

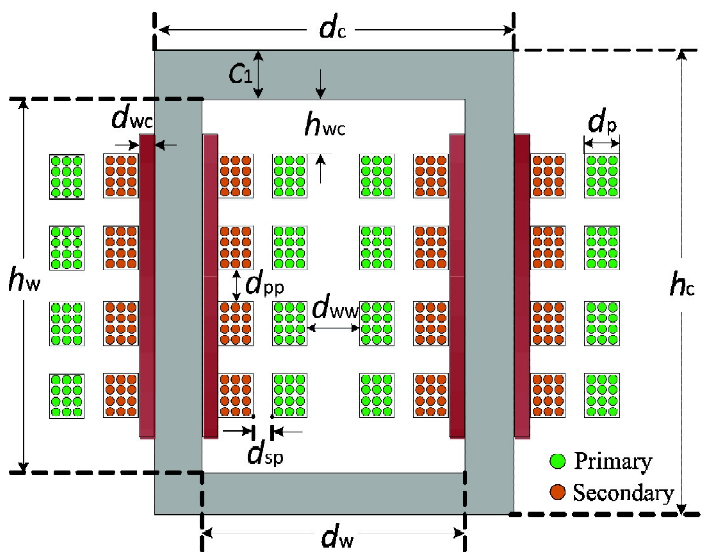

Figure 7: The Schematic diagram of medium-frequency transformer modeling

nanocrystalline alloy, which has advantages of lower losses and higher saturated flux density (1.25 T). Litz wire windings are used to reduce the skin effect on winding losses at high frequencies. Subsequently, the rated parameters of large-capacity MFT model are listed in Table II.

1kV/10kHz MFTs are usually connected in series as a component inside 10 kV PET, and the main insulation level of MFT should be designed according to the highest system voltage of 10 kV. According to the breakdown properties of insulating materials at high frequency, the withstand voltage of the film insulating material is not less than 40 kV/mm at10 kHz, and the winding insulation level of 4.1 kV can be achieved by using an insulating film of 0.14 mm, and finally formed litz wire winding with a diameter of 17 mm. Meanwhile, epoxy resin is used as a pad between the secondary winding and the core. According to the flashover test results, the flashover voltage of the epoxy casting resin under electric stress of 10 kHz is about 12.65kV/10mm, so the creepage distance from the edge of the secondary winding to the core should be no less than 10 mm at the highest system voltage of 10 kV to ensure that no flashover occurs between the secondary winding and the core. In addition, there is an insulation problem of air gaps between the primary and secondary windings. According to the high-frequency breakdown test results of air gaps, the breakdown field strength of air at 10 kHz is about 1.5 kV/mm. Since high-frequency breakdown will cause serious accidents, the air gap can be designed with a 50% margin at high frequencies, and the airway width can be higher than 10 mm to fully ensure the reliability of the main insulation. The insulation size mentioned above is the minimum value, and the insulation size can be appropriately increased during the design of the heat dissipation structure, taking into account the loss and heat dissipation of each part.

Table II
The Rated Parameters of Large-Capacity MFT

Rated Capacity	*Rated Frequency*	*Primary Voltage*	*Secondary Voltage*	*Temperature Rise*
200 kVA	10 kHz	1 kV	0.8 kV	≤ 80 K

B. Core Losses

There are several approaches to core loss estimation, among which the waveform coefficient Steinmetz equation (WCSE) proposed by W. Shen [11] has applicability for the core loss estimation under high frequency non-sinusoidal signals.

$$p_c = F_w K_m f^{\alpha} B_m^{\beta} \tag{1}$$

where p_c is the loss density; F_w is the waveform coefficient of the core; B_m is the maximum magnetic flux density; K_m, α and β are key constants related to frequency and core material.

For the rectangular signal, the waveform coefficient F_w can be calculated as:

$$F_w = \frac{\pi}{4}(2 - D) \tag{2}$$

where D is the duty ratio, and its value is 1 for the bipolar square wave signal, which is the operating condition of MFTs.

Meanwhile, the maximum magnetic flux density of MFT can be calculated by equation (3).

$$B_m = \frac{U_p}{k_f k_c n \cdot S} \tag{3}$$

where U_p is the effective voltage value of the primary winding; k_f is the waveform coefficient of the primary winding, and its value is 4 for square wave signal; k_c is the lamination coefficient of the core, and its value is 0.8 for the lamination process of the nanocrystalline core used in this paper; n is the number of turns of the primary winding; S is the cross-sectional area of the core.

The core losses of nanocrystalline alloy are related to the voltage frequency and the maximum magnetic flux density. Fig. 8 shows the *B-P* fitting curve at the frequency of 10 kHz, from which the *B-P* characteristic equation can be calculated:

$$p_c = 25.94 \cdot B_m^{\ 2.342} \tag{4}$$

Since the linearity of the fitting curve is 0.9973, it can be considered that the calculated results according to the *B-P* characteristic equation are close to the actual core losses.

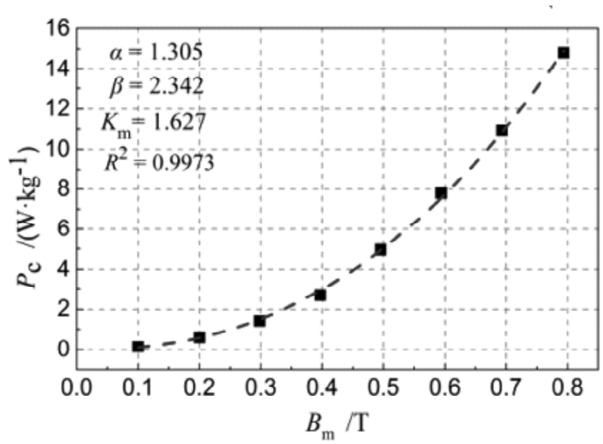

Figure 8: The *B-P* characteristic fitting curve of nanocrystalline core at 10 kHz

C. Winding Losses

The Dowell model is widely used in the calculation and analysis of the foil winding losses under high frequency. The core idea of the Dowell model is to establish a simplified model of the transformer, and then derive the calculation formula for the winding losses using the electromagnetic equations. After the analytical derivation, the calculation formula of foil winding losses can be expressed as:

$$P_w = \sum_{i=1}^{m} P_\sigma = I^2 \frac{m}{\sigma' \delta \cdot h_w}\left[P_1 + \frac{2}{3}(m^2 - 1)P_2\right] \tag{5}$$

where P_w is the winding loss; P_σ is the power loss of the single-layer winding; $m$is the number of layers of the winding; I is the effective current value; δ is the skin depth; σ´ is the equivalent conductivity of copper, which is about 4.29×10^7 S/m for long-foil windings at 100°C; h_w is the height of the core window; P_1 is the skin effector, and P_2 is the proximity effect factor.

The skin depth δ, the skin effector P_1 and the proximity effect factor P_2 can be calculation with the following:

$$\delta = \sqrt{\frac{\rho}{\pi \mu f}} \tag{6}$$

$$P_1 = \frac{\sinh(2\Delta) + \sin(2\Delta)}{\cosh(2\Delta) - \cos(2\Delta)} \tag{7}$$

$$P_2 = \frac{\sinh(\Delta) - \sin(\Delta)}{\cosh(\Delta) + \cos(\Delta)} \tag{8}$$

where ρ is the resistivity; μ is the magnetic permeability of the copper; Δ is equal to d/δ, where d is the radius of copper wires.

Nevertheless, the original Dowell model is only suitable for long foil windings. In order to extend the Dowell model to the calculation of losses in other types of windings such as circular windings, square windings, and short-foil windings, the porosity coefficient η is introduced to convent the conductivity of the windings, as shown in Fig. 9.

In terms of the circular litz wire windings, the porosity coefficient η and equivalent conductivity σ' can be calculated:

$$\eta_1 = \frac{4d_s}{h_s} = \frac{2\times\sqrt{\pi}d_r}{h_s} \tag{9}$$

$$\eta_2 = \frac{h_s}{h_w} \tag{10}$$

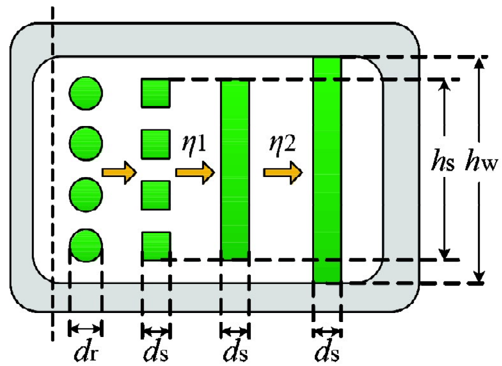

Figure 9: The conversion of different forms of the windings in the core window based on the Dowell analysis model

$$\sigma' = \eta_1 \cdot \eta_2 \cdot \sigma \tag{11}$$

where d_r is the diameter of circular winding; d_s is the equivalent diameter of square winding with the same cross-section.

D. Surface Heat Transfer Coefficients

There are three forms of heat dissipation for MFT, including the conduction, the convection over hot-plate, and the radiation. Among them, since the heat conduction and radiation can be analyzed based on the basic properties of the materials and a given structure, the setting of surface heat transfer coefficients of the heat convection determines whether the simulation results of the temperature field are accurate. There are nine types of surface heat dissipation of MFT, which are listed below.

Table III
Different types of the Surface Heat Dissipation

Convection Interface	*Facing Up*	*Facing Down*	*Vertical Surface*
Core-Fluid	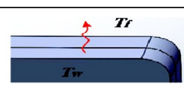	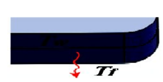	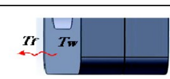
Primary-Fluid	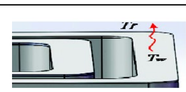	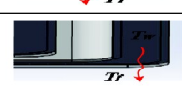	
Secondary-Fluid	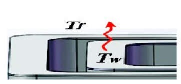	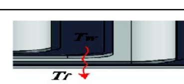	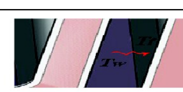

In terms of convection with the heat sink facing up or facing down, the surface heat transfer coefficient can be calculated as:

$$h = N_u \cdot \frac{\lambda L}{S} \tag{12}$$

where h is the heat transfer coefficient; λ is the thermal conductivity of the fluid; L is the circumference; S is the heat sink area; N_u is the Nusselt number, which is calculated as:

$$N_u = A(G_r \cdot P_r)^m \tag{13}$$

where G_r is called the Grashof Number, and P_r is called the Prandtl Number. G_r and P_r can be calculated as equation (14)-(15). Meanwhile, A and m are constants which are related to the calculation result of $G_r \cdot P_r$, as listed in Table IV.

$$G_r = \frac{g\left(\frac{S}{L}\right)^3 \gamma \cdot \Delta t}{v^2} \tag{14}$$

$$P_r = C_p \cdot \frac{v}{\lambda} \tag{15}$$

where g is the gravitational acceleration; Δt is the temperature difference between surface and the fluid; v is the kinematic viscosity; C_p is the specific heat capacity; γ is volume expansion coefficient of the fluid, which can be calculated as:

$$\beta = \frac{1}{T} = \frac{2}{T_f + T_w} \tag{16}$$

In terms of the vertical flow-through heat transfer, the surface heat transfer coefficient can be calculated as:

$$h = N_u \cdot \frac{\lambda}{H} \tag{17}$$

where H is the height of the vertical heat sink surface, and the calculation of N_u is the same as the equation (14). Nevertheless, G_r is calculated by equation (18) for vertical heat transfer.

$$G_r = \frac{gH^3 \gamma \cdot \Delta t}{v^2} \tag{18}$$

Table IV
Reference Values for Parameters *A* and *M*

Hot Direction	$G_r \cdot P_r$	*State of the fluid*	*A*	*m*
Vertical	10^4~10^9	laminar flow	0.59	0.25
	10^9~10^{13}	turbulent flow	0.12	0.33
Facing Up	2×10^4~8×10^6	laminar flow	0.54	0.25
	8×10^6~8×10^{11}	turbulent flow	0.15	0.33
Facing Down	10^5~10^{11}	laminar flow	0.58	0.20

IV. OPTIMAL DESIGN OF HEAT DISSIPATION

Insulation performance and volume are important factors to consider when designing the heat dissipation structure of MFTs. Since the MFT designed in this paper will be used in a PET with the rated voltage of 10 kV, the insulation level between the core and windings should be calculated with reference to the maximum operating voltage of the system. Meanwhile, the inter-turn insulation level inside the windings can be obtained by referring to Table I. This part firstly designs the heat dissipation structure under natural air-cooling conditions, and then gradually reduces the volume of MFT under the premise of ensuring the insulation performance, and designs reasonable heat dissipation methods to meet different application scenarios.

A. Natural Air-Cooling Heat Dissipation

Fig. 10 shows a 1/2 section of a three-dimensional model of a dry-type MFT. Since the heat dissipation performance under air-cooling conditions is determined by the height and area of the heat dissipating surface, the structural parameters of the MFT are set after repeated calculations, as listed in Table V. Definitions of structural parameters have been shown in Fig. 7.

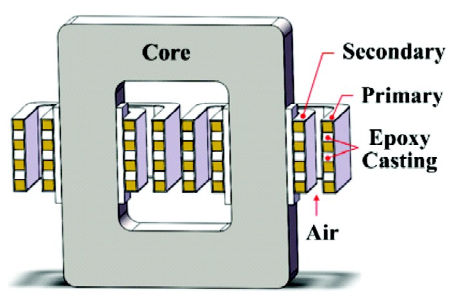

Figure 10: 1/2 section of a three-dimensional model of the natural air-cooled MFT

Table V
The Structural Parameters of MFT

Parameters	C_1	d_c	h_c	d_w	h_w
Settings	90 mm	360 mm	420 mm	180 mm	240 mm
Parameters	d_{wc}	h_{wc}	d_{pp}	d_{ww}	d_{sp}
Settings	10 mm	63.5 mm	15 mm	42 mm	25 mm

Subsequently, the surface heat transfer coefficients h of different parts of the MFT can be calculated, as listed in Table VI. After calculation based on the equation (1) to (11), the core loss is 179.9 W, while the loss of windings is 224.2 W, which together with the thermal properties of materials listed in Table VII as the input values for the finite element simulation of temperature distribution. Meanwhile, the boundary condition for the temperature field simulation is set to:

$$-\lambda \cdot \left(\frac{\partial T}{\partial x}\right)_w = h(T_w - T_f) \tag{19}$$

where $\partial T/\partial x$ is the rate of change of fluid temperature in the normal direction of the convection interface.

Table VI
Calculation Results of Surface Heat Transfer Coefficients

Heat Transfer Coefficients W/(m^2·C)	*Facing Up*	*Facing Down*	*Vertical Surface*
Core-Air	8.431	4.498	5.349
Primary-Air	11.338	8.018	6.707
Secondary-Air	11.519	8.151	6.707

Table VII
The Basic Thermal Properties of The MFT Materials

Materials	*Density kg/m^3*	*Heat Capacity J/(kg·K)*	*Conductivity W/(m·K)*
Nanocrystalline	7180	450	8
Copper	8954	383.1	386
Casting Resin	980	1511	0.2
Air	1.2	1005.6	0.025

The temperature distribution of 1/2 MFT model under natural air-cooling is shown in Fig. 11(a). For numerical analysis, five characteristic temperature interfaces are selected to insert the boundary probes, as shown in Fig.11(b).

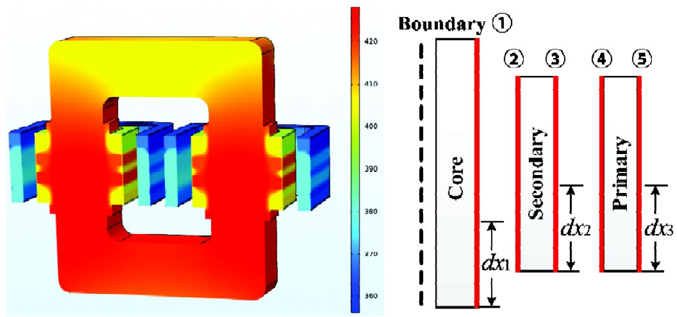

Figure 11: (a) The temperature distribution of the 1/2 MFT model. (b) The boundary probes of characteristic temperature interfaces

Fig. 12 shows the steady-state temperature rises of the core and windings. It can be seen from Fig. 12 that the temperature of the lower half the core is much higher than that of the upper half because the upward surface heat transfer coefficient is about 1.87 times the downward heat transfer coefficient. In addition, since the heat of secondary winding is mainly carried away by air convection on single side while the heat of primary winding can be dissipated by the air convection on both sides, the temperature rise of secondary winding is 40~50 K higher than that of primary winding. The core and the secondary winding become the focus of heat dissipation optimal design.

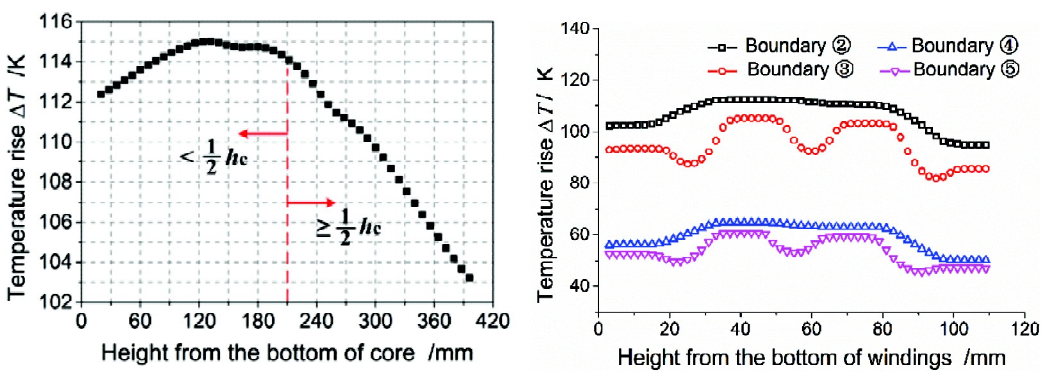

Figure 12. (a) The temperature rises of the core. (b) The temperature rises of the primary winding and the secondary winding

Since the temperature rises of the core and the secondary winding are 100~115 K, it is necessary to properly design the thickness, height and number of the heat sink fins to control the steady-state temperature rise within the allowable range of the large-capacity MFT. Fig. 13 shows the definition of the size parameters for the upper and lower heat sink fins. After several times of simulation calculations, the reasonable parameters of the heat sink fins are finally formulated, as listed in Table VIII. Meanwhile, the temperature distribution is shown in Fig. 14.

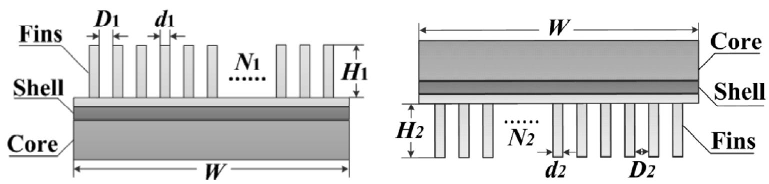

Figure 13: Definition of the size parameters for the upper and lower heat sink fins

Table VIII
The Parameters of Upper and Lower Heat Sink Fins

Parameters	W_1	N_1	H_1	D_1	d_1
Settings	360 mm	26	70 mm	8.5 mm	5.0 mm
Parameters	W_2	N_2	H_2	D_2	d_2
Settings	360 mm	35	70 mm	6.0 mm	4.0 mm

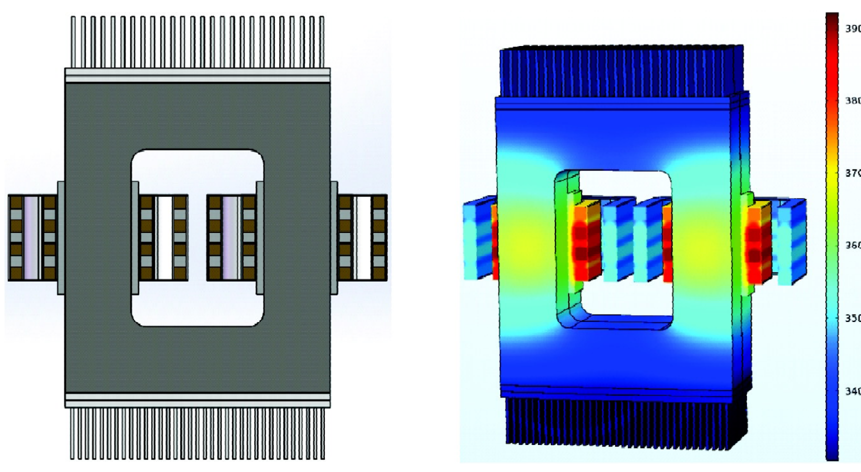

Figure 14: Temperature distribution of the MFT after the heat sink fins are added

Fig. 15 shows the temperature rises of the core and windings after the heat sink fins are installed. It can be seen from Fig. 15 that the steady-state temperature rise of the upper and lower half of the core tends to be symmetrical due to the optimal design in the number and thickness of the heat sink fins, and the maximum temperature rise of the core is 57.2 K, which is about 58 K lower than that before the heat sink fins are installed. Moreover, the temperature rise of the secondary winding is reduced by 35 K due to the heat conduction between the core and winding. Therefore, the above insulation structure and the parameter settings of heat sink fins can ensure that the steady-state temperature rise of MFTs is limited to the allowable range.

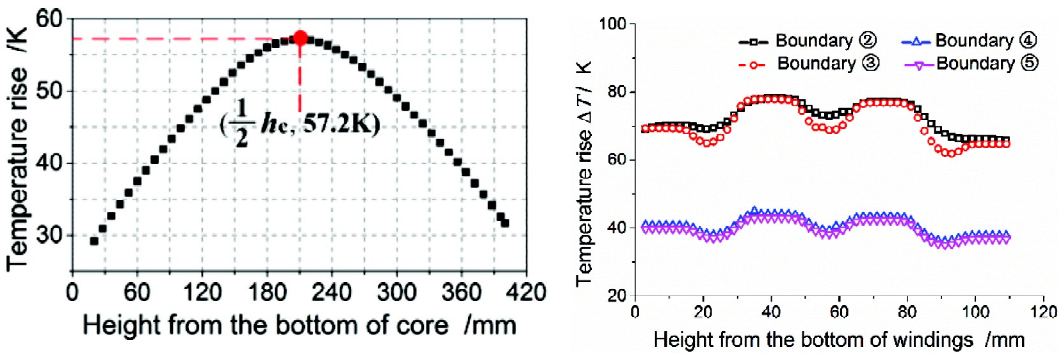

Figure 15: (a) Temperature rises of the core after the heat sink fins are added. (b) Temperature rises of the windings after the heat sink fins are added

B. Forced Air-Cooling Heat Dissipation

In fact, in the above insulation structure design, a certain size is reserved to increase the heat dissipation area, so that the purpose of cooling is achieved under the natural air-cooling method. However, the MFT with smaller volume is required in some specific applications. While reducing the volume, it is also necessary to ensure the insulation performance of the MFT, so Table IX lists the minimum insulation size of 200 kVA/10 kHz MFT. In order to keep the steady-state temperature rise within an allowable range in the smaller volume, a forced air-cooling heat-dissipation method is proposed. Fig.16(a) is the temperature distribution without forced air-cooling. The results show that the temperature of the secondary winding is 470~503K, which is 157~190 K higher than the ambient temperature (40 °C). In order to make the maximum temperature rise of the MFT lower than 80 K, the forced air-cooling is used to continuously increase the velocity of air between the windings. Then, the variations of the maximum temperature values of the core, the primary winding and the secondary winding with the velocities of air are obtained, as shown in Fig.17. It can be seen from Fig. 17 that the temperatures of the primary winding and secondary winding decrease as the velocity of air increases due to the enhancement of heat convection, and the temperature of core is also decreased because of heat conduction. When the velocity of air flow is 1.6 m/s, it is ensured that the maximum partial temperature rises of MFTs are below 80 K, which is within the allowable temperature range during the long-term operations.

Table IX
The Minimum Insulation Size of 200 kVA/10 kHz MFT

Parameters	C_1'	d_c'	h_c'	d_w'	h_w'
Settings	60 mm	260 mm	270 mm	140 mm	150 mm
Parameters	d_{wc}'	h_{wc}'	d_{pp}'	d_{ww}'	d_{sp}
Settings	5 mm	31.5 mm	5 mm	16 mm	15 mm

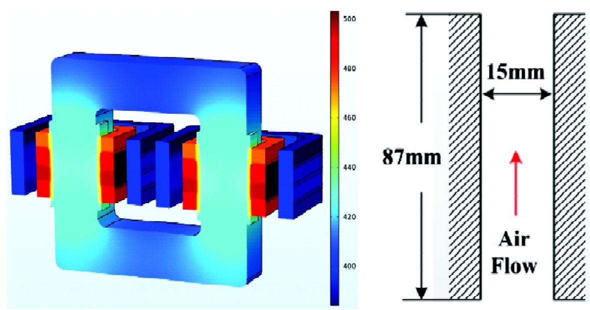

Figure 16: (a) The temperature distribution of smaller size of MFT without forced air-cooling. (b) Schematic diagram of the forced air-cooling process

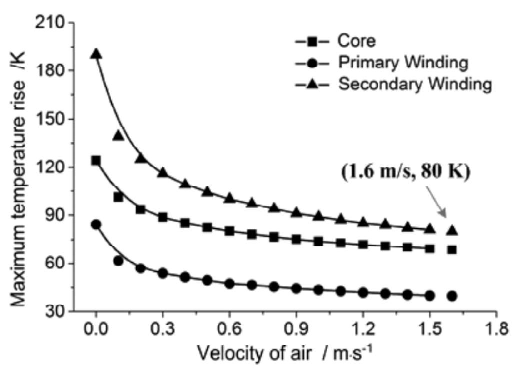

Figure 17: Variations of the maximum temperature rises of the core, primary winding and secondary winding with different velocities of air

V. CONCLUSION

The insulation structure of MFT were designed based on the high-frequency insulation tests on the gas-solid system, which have shown that the breakdown and flashover voltages drop remarkably with the increase of frequency. Meanwhile, the breakdown damages of dielectrics are more serious as the frequency increases. Thus, the thicknesses of airgaps and solid materials should be increased in the insulation design of MFTs.

A natural air-cooled heat dissipation structure has been designed based on the accurate calculation of core loss, winding loss and surface heat dissipation coefficients. The simulation results have shown that the temperature of the lower half the core is much higher than that of the upper half, and the temperature rise of secondary winding is 40~50 K higher than that of primary winding due to the heat of secondary winding is mainly dissipated by air convention on single side. Therefore, the numbers and thicknesses of heat sink fins were designed to enhance heat dissipation. After installing the fins, the steady-state temperatures of the upper and lower half of the core tends to be symmetrical, and the maximum temperature is about 58 K lower than that before the fins are installed. Meanwhile, the temperature of secondary winding is reduced by 35 K due to the enhancement of heat conduction between the core and winding.

In addition, a forced air-cooled heat dissipation method has been proposed due to the temperature rise has been reached 157~190 K at the minimum volume (≈ 0.02 m^3) that ensures insulation performance. When the velocity of air is 1.6 m/s, it is ensured that the partial temperature rises of the MFT model are below 80 K, which is within the allowable operating limits of MFT. Developed optimal design method of heat dissipation structure considering insulation performance will be further verified by MFT prototypes in our future studies.

VI. ACKNOWLEDGMENT

This paper is based upon work supported by the National Key R&D Program of China (Grant No. 2017YFB0903902).

REFERENCES

[1] S. Xu, A. Q. Huang, and R. Burgos. (2013). “Review of solid-state transformer technologies and their application in power distribution systems,” *IEEE J. Emerging and Sel. Topics in Power Electron*., 1(3), 186-198.

[2] I. Syed and V. Khadkikar. (2017). “Replacing the grid interface transformer in wind energy system with solid-state transformer,” *IEEE Trans. Power Syst.*, 32(3), 2152-2160.

[3] M. Liserre, G. Buticchi, M. Andresen, *et al*. (2016). "The smart transformer: impact on the electric grid and technology challenges," *IEEE Ind. Electr. Mag.*, 10(2), 46-58.

[4] M. Leibl, G. Ortiz, and J. W. Kolar. (2017). "Design and experimental analysis of a medium-frequency transformer for solid-state transformer applications," *IEEE J. Emerging and Sel. Topics in Power Electron.*, 5(1), 110-123.

[5] S. Baek, Y. Du, G. Wang, *et al*. (2010). "Design considerations of high voltage and high frequency transformer for solid state transformer application," in *36th Annual Conf. IEEE Industrial Electron. Soc.*, Glendale, USA, 421–426.

[6] P. Huang, C. X. Mao, D. Wang, *et al*. (2017). "Optimal design and implementation of high-voltage high-power silicon steel core medium-frequency transformer," *IEEE Trans. Industrial Electron.*, 64(6), 4391-4401.

[7] M. Mogorovic and D. Dujic. (2017). "Thermal modelling and experimental verification of an air-cooled medium frequency transformer," in *Proc. 19th Eur. Conf. Power Electron. Appl.*, Warsaw, Poland, 1–10.

[8] Y. Zhao, G. Zhang, R. Guo, *et al*. (2019). "The breakdown characteristics of thermostable insulation materials under high-frequency square waveform," *IEEE Trans. Dielectr. Electr. Insul.,* 26(4), 1073-1080.

[9] J. Reinert, A. Brockmeyer, and R. W. A. A. De Doncker. (2001). "Calculation of losses in ferro-and ferrimagnetic materials based on the modified Steinmetz equation," *IEEE Trans. Industry Appl.,* 37(4), 1055-1061.

[10] K. Venkatachalam, C. R. Sullivan, T. Abdallah, *et al*. (2002). "Accurate prediction of ferrite core loss with non-sinusoidal waveform s using only Steinmetz parameters," in *Proc. 2002 IEEE Workshop on Computers in Power Electron.*, Mayaguez, USA, 36–41.

[11] W. Shen, F. Wang, D. Boroyevich, *et al*. (2008). "Loss characterization and calculation of nanocrystalline cores for high-frequency magnetics applications," *IEEE Trans. Power Electron.,* 23(1), 475-484.

[12] P. L. Dowell. (1966). "Effects of eddy currents in transformer windings," *Proc. Inst. Electr. Engineers,* 113(8), 1387-1394.

[13] M. Mogorovic and D. Dujic. (2019). "100 kW, 10 kHz medium-frequency transformer design optimization and experimental verification," *IEEE Trans. Power Electron.,* 34(2), 1696-1708.

[14] G. Ortiz, M. Leibl, J. W. Kolar, *et al*. (2013). "Medium frequency transformers for solid-state transformer applications-design and experimental verification," in *Proc. International Conf. Power Electron. and Drive Syst.*, Kitakyushu, Japan, 1285–1290.

[15] T. Kjellqvist, S. Norrga, and S. Ostlund. (2004). "Design considerations for a medium frequency transformer in a line side power conversion system," in *Proc. 35th Annual Power Electron. Specialists Conf.*, Aachen, Germany, 2572–2576.

[16] T. Liu, Q. Li, X. Huang, *et al*. (2018). "Partial discharge behavior and ground insulation life expectancy under different voltage frequencies," *IEEE Trans. Dielectr. Electr. Insul.,* 25(2), 603-613.

[17] J. H. Mason. (1992). "Effects of frequency on the electric strength of polymers," *IEEE Trans. Dielectr. Electr. Insul.,* 27(6), 1213-1216.

[18] E. Kuffel, S. Grzybowski, and R. B. Ugarte. (1972). "Flashover across polythelene and tetrafluoroethylene surfaces in vacuum under direct, alternating and surge voltages of various waveshapes," *J. Phys. D, Appl. Phys.,* 5(3), 575-579.

[19] K. Elanseralathan, M. Joy, and G. R. Nagabhushana. (2000). "Breakdown of solid insulating materials under high frequency high voltage stress," in *Proc. 6th Int. Conf. on Properties and Applications of Dielectric Materials*, Xi'an, China, 999–1001.

[20] *Insulation Coordination for Equipment within Low-Voltage Systems-Part 4: Consideration of High-Frequency Voltage Stress,* IEC Standard 60664-4, 2005.